

## Prediction System of Cloud Distribution Image Using Fully Convolutional Networks

Koki Akiyama, Hiroshi Suzuki, Takahiro Kitajima and Takashi Yasuno

Graduate School of Sciences and Technology for Innovation, Tokushima University  
2-1 Minami-Josanjima, Tokushima 770-8506, Japan  
E-mail: akiyama-k@ee.tokushima-u.ac.jp  
{suzuki.hiroshi, yasuno.takashi}@tokushima-u.ac.jp

### Abstract

In this paper, we propose a cloud distribution prediction model in which fully convolutional networks are used to improve the prediction accuracy for photovoltaic power generation systems. The model learns the cloud distribution from meteorological satellite images and predicts the cloud image 60 min later. We examined the applicability of Day Microphysics RGB as input to the cloud image prediction model. Day Microphysics RGB is a type of RGB composite image based on the observation image of Himawari-8. It is used for daytime cloud analysis and can perform detailed cloud analysis, for example, the discrimination of cloud areas such as upper and lower clouds. The performance of the proposed method is evaluated on the basis of the root mean square error of the prediction and ground truth images.

### 1. Introduction

In recent years, with the increase in the number of photovoltaic (PV) systems being used, there has been concern about adverse effects on the electric power system as a result of fluctuations of the PV output. Gathering the PV output is important for the stable and efficient operation of the electric power system. The PV output can be calculated from the level of solar radiation, and prediction methods of the amount of solar radiation using satellite cloud images have been proposed [1,2]. In this paper, we propose a method of cloud distribution prediction using satellite cloud images and a fully convolutional network (FCN). FCN has high image analysis capability. We expect to improve the prediction accuracy by using Day Microphysics RGB as input to the prediction model. Day Microphysics RGB is a composite RGB image based on observation images obtained from Himawari-8. It is used for cloud analysis during the daytime and can perform detailed cloud analysis, for example, the discrimination of cloud areas such as upper and lower clouds. Cloud information in the daytime is important in predicting visible cloud images. Therefore, we compare and examine the effect of prediction using Day Microphysics RGB as input to the pre-

dition model. The performance of the prediction model is evaluated on the basis of the root mean square error (RMSE) of the prediction and ground truth images. The prediction performance of the proposed model is also evaluated by comparison with two other models with different inputs.

### 2. Cloud Image Prediction Model

In this paper, we propose a cloud image prediction model using FCN, which inputs satellite images observed by the Himawari-8 weather satellite and predicts cloud images 60 min later. Figure 1 shows the architecture and parameters of the proposed model.

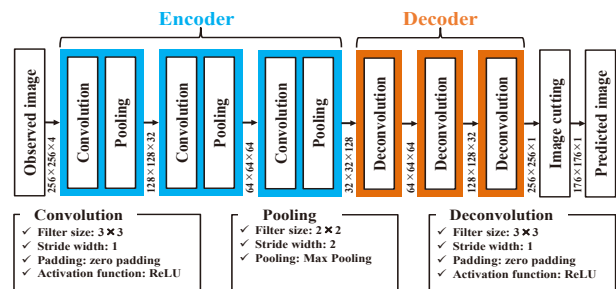


Figure 1: Network architecture of prediction model

The prediction model is composed of FCN with an encoder-decoder architecture, which is a type of convolutional neural network consisting only of convolutional layers, and it can generate images based on feature extraction from images. The proposed model has three convolutional layers, three pooling layers, and three deconvolutional layers. The convolutional and pooling layers extract features from input images as an encoder. The deconvolutional layers perform deconvolution and thus function as a decoder and then generate prediction images. This architecture is expected to provide predictions while preserving the information contained in the input images.

The  $i$ -th output value of unit  $z_{xy}^{ij}$  at position  $(x, y)$  in the

$j$ -th feature map with the filter of  $P_i \times Q_i$  is given by

$$z_{xy}^{ij} = f \left( \sum_{k=0}^{K-1} \sum_{p=0}^{P_i-1} \sum_{q=0}^{Q_i-1} z_{(x+p)(y+q)k}^{(i-1)j} h_{pq}^{kij} + b_{ij} \right) \quad (1)$$

where  $f$  is the activation function,  $K$  is the number of channels in the previous layer,  $h$  is the pixel value of the filter, and  $b$  is the bias.

### 3. Cloud Image Data

The input of the model is satellite images observed at 10-min intervals by Himawari-8 [3,4]. Himawari-8 observes 16 bands: three visible, three near-infrared, and ten infrared. Figure 2(a) is a visible image of the 0.64  $\mu\text{m}$  band (band 3), which shows the reflectance of sunlight by clouds and the Earth's surface. Figures 2(b) and 2(c) are near-infrared (band 6) and infrared (band 13) images, respectively. The image around Shikoku Island, which is the prediction target, is  $256 \times 256$  pixels and the resolution is about 1 km/pixel. The output image of the model is evaluated and trained only the central  $176 \times 176$  pixels, taking into account the movement of the clouds due to wind. Datasets of observed cloud images were created for training, validation, and evaluation using the images taken in August 2016, August 2017, and August 2018, respectively.

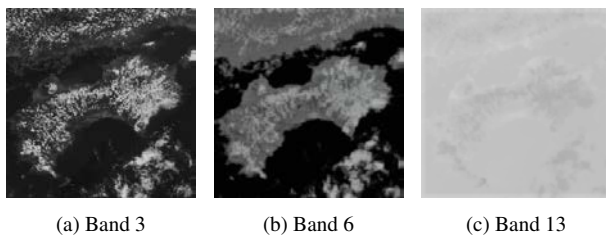


Figure 2: Examples of satellite image (Himawari-8)

It is difficult to analyze details from all the images of the 16 bands observed by Himawari-8. To solve this problem, the use of RGB composite images has been proposed; such images are superimposed using multiple band images in accordance with applications such as daytime cloud analysis, night-time cloud analysis, and air mass analysis [5]. Day Microphysics RGB is the RGB composite of images of three bands observed by Himawari-8: band 4 (0.86  $\mu\text{m}$ ) as the red channel, the sunlight reflection component extracted from band 7 (3.9  $\mu\text{m}$ ) as the green channel, and the inverse of band 13 (10.4  $\mu\text{m}$ ) as the blue channel. It can be used to identify various cloud regions, such as cumulus, ice, and water clouds, during the day. Therefore, it is expected to improve the prediction accuracy of visible satellite images by using it as input.

**Band 4** Band 4 yields the optical thickness of the cloud, with thinner clouds appearing darker and thicker clouds appearing brighter.

**Solar reflection from band 7** Band 7 usually shows two types of energy during the day: the energy emitted directly from the Earth's surface and clouds, and the energy of reflected sunlight. Therefore, we can obtain only the reflection of sunlight by removing the energy directly emitted from the Earth's surface and clouds from band 7. Band 13 corresponds to the energy emitted directly from the Earth's surface and clouds. Therefore, by subtracting band 13 from band 7, we can obtain images of only the reflected components of sunlight [6]. The solar reflection from band 7 is highly dependent on the phase and size of cloud particles. It can also identify the type of cloud.

**Inverse of band 13** The inverse of band 13 is dependent on the brightness temperature and provides cloud height information.

Figures 3(a) to 3(c) show images of each channel of Day Microphysics RGB. The composite Day Microphysics RGB is shown in Fig. 3(d).

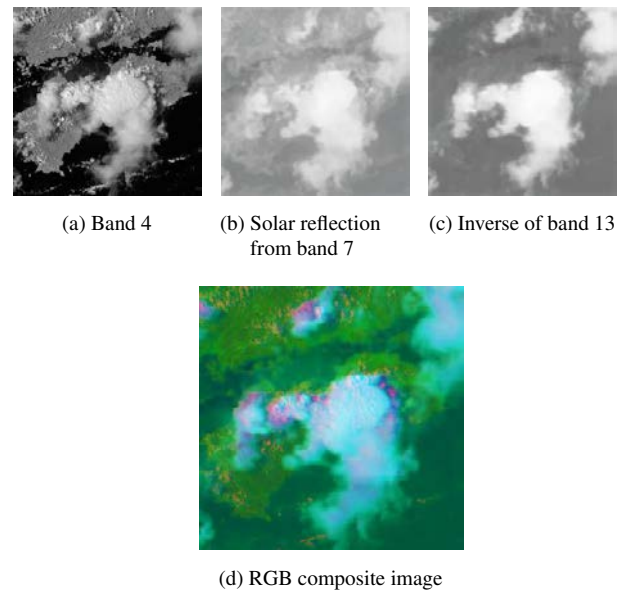


Figure 3: Day Microphysics RGB

### 4. Evaluation Method

The prediction performance of the proposed model is evaluated by comparison with two other models with different inputs: raw model and unused model. Table 1 shows the input conditions of the three models. The input of the raw model is raw image information of bands 3, 4, 7, and 13, which correspond to the input of the proposed model. It can be considered

Table 1: Input conditions of the models

	Input 1	Input 2	Input 3	Input 4
Proposed model	Band 3	Band 4	Band 7 (sol)	Band 13 (inv)
Raw model	Band 3	Band 4	Band 7	Band 13
Unused model	Band 3	-	-	-

Table 2: Learning conditions

Loss function	Root mean square error (RMSE)		
Optimizer	Adam	$\alpha$	0.001
		$\beta_1$	0.9
		$\beta_2$	0.999
		$\epsilon$	$1.0 \times 10^{-8}$
Batch size	8		

that the raw model has the same information as the proposed model. The input of the unused model is only visible image band 3.

Table 2 shows the learning conditions. Each network is trained for 100 epochs using the training dataset, and the error relative to the validation dataset is calculated for each epoch.

The model at the epoch with the smallest error is used as the prediction model. The root mean square error (RMSE) in Eq. (2) is used as the prediction error.

$$RMSE = \sqrt{\frac{1}{mnc} \sum_{k=0}^{c-1} \sum_{y=0}^{n-1} \sum_{x=0}^{m-1} \{T(x, y, k) - P(x, y, k)\}^2} \quad (2)$$

Here,  $m$  and  $n$  are the height and width of the evaluation area, respectively.  $c$  is the number of channels and  $T$  and  $P$  are the pixel values of the ground truth and prediction images, respectively. A smaller RMSE indicates a more accurate prediction.

## 5. Prediction Results

Table 3 shows the average RMSEs of all pixels over the evaluation period for the three models. The proposed model exhibits the highest accuracy. Figure 4(a) shows the average RMSE on each day, and Fig. 4(b) shows the average RMSE of each hour for one month.

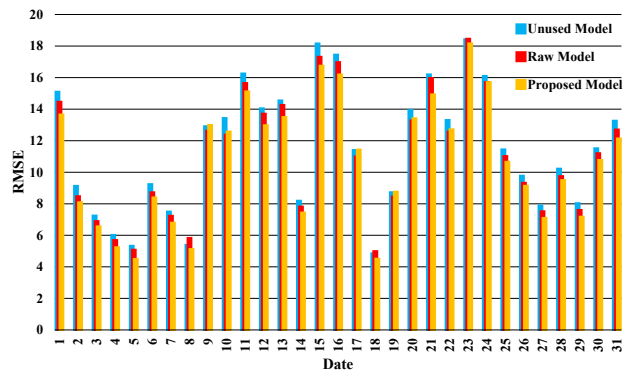
From Fig. 4(a), we can see that the proposed model has improved prediction accuracy on most of the days. From Fig. 4(b), it is confirmed that the improvement is due to the contribution of what from 8 am to 1 pm and 6 pm and 7 pm. In addition, the prediction accuracy was considerably improved at the time of sunset (6 pm and 7 pm), which is a difficult time to predict from only band 3 because of the lack of cloud

Table 3: Average RMSEs of the three models

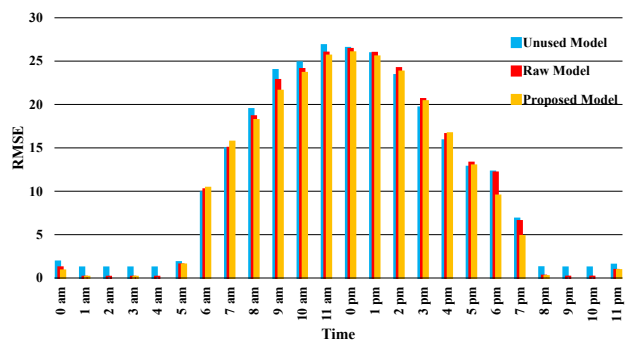
	Unused model	Raw model	Proposed model
RMSE	11.375	10.977	10.634

information. This means that the cloud information of thickness, height, and structure contained in the Day Microphysics RGB image is useful for visible image prediction at times when cloud information is lacking. Therefore, the usefulness of the Day Microphysics RGB image in visible image prediction was confirmed. Table 3 confirms that the prediction accuracy can be improved by inputting images that have been processed in accordance with the prediction target, rather than inputting raw observation satellite images.

However, from 2 pm to 5 pm, the unused model has the highest prediction accuracy. Here, to examine the prediction and ground truth images from 2 pm to 5 pm, examples of the prediction and ground truth images for the proposed model and unused model are shown in Fig. 5. Figure 5 shows that the proposed model tends to predict clouds in detail, whereas the unused model tends to predict clouds in a blurred manner, which is the reason why the unused model has a smaller prediction error from 2 pm to 5 pm. In addition, the afternoon sun is strong during this time range in summer, and detailed information on clouds can be obtained from only band 3, which corresponds to the reflection of sunlight. However, by adding the cloud information of height, thickness, and structure to the input, more detailed cloud distribution prediction becomes possible, and further additional information is expected to improve the prediction accuracy in the future.



(a) Average RMSE on each day: August, 2018



(b) Average RMSE of each hour for one month: 0 am is midnight and 0 pm is noon.

Figure 4: Error between prediction and ground truth images

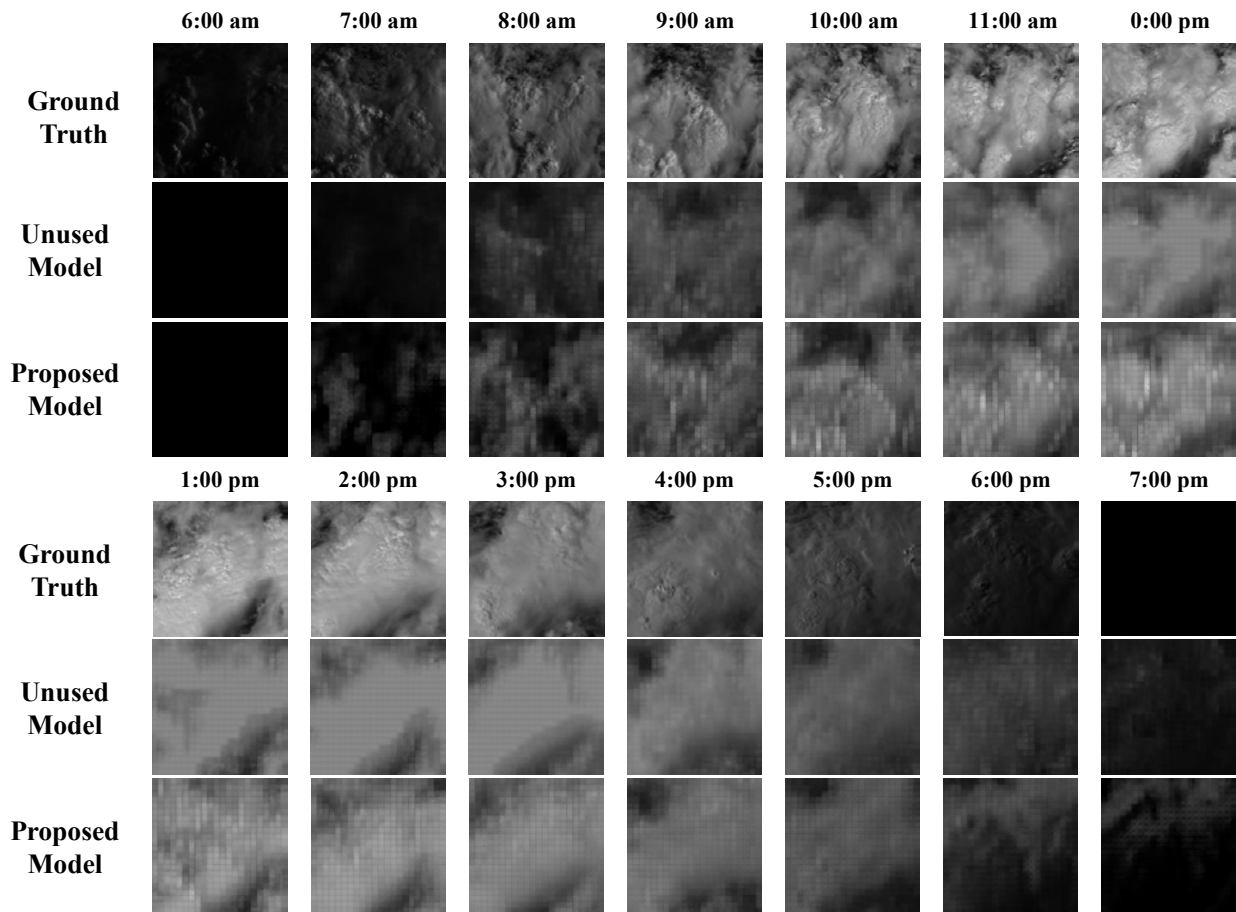


Figure 5: Predicted and ground truth images for each input every hour from 6:00 am to 7:00 pm (UTC+09:00) on August 15, 2018

## 6. Conclusions

We proposed the cloud prediction model in which FCN is used to predict the cloud distribution 60 min later. The results of several prediction analyses using observed satellite image data confirmed the following:

- The prediction accuracy of visible satellite images is improved by adding Day Microphysics RGB to the input.
- The preprocessing of meteorological satellite images is important for improving the prediction accuracy.

A future task is to verify the general applicability of the proposed model by performing predictions for all months.

### Acknowledgment

Himawari-8 gridded data are distributed by the Center for Environmental Remote Sensing (CEReS), Chiba University, Japan.

### References

- [1] S. Kajikawa, H. Suzuki, T. Kitajima, A. Kuwahara, T. Yasuno and K. Takigawa: Nowcasting of solar radiation using CNN with changing input range of meteorological satellite image, 2020 RISP International Workshop on Nonlinear Circuits, Communications and Signal Processing, No. 29PM2-1-5, pp. 210-213, 2020.
- [2] K. Takigawa: Development and practical use of estimation and prediction system of PV, Shikoku Research Institute, Research Report, No. 104, pp. 27-39, 2016.
- [3] H. Takenaka, T. Sakashita, A. Higuchi and T. Nakajima: Development of geolocation correction for geostationary satellite observation by a phase-only correlation method using a visible channel, *Remote Sensing*, Vol. 12, No. 15, p. 2472, 2020.
- [4] Y. Yamamoto, K. Ichii, A. Higuchi and H. Takenaka: Geolocation accuracy assessment of Himawari-8/AHI imagery for application to terrestrial monitoring, *Remote Sensing*, Vol. 12, No. 9, p. 1372, 2020.
- [5] Japan Meteorological Agency: Basics of meteorological satellite observation and application of Himawari-8 multi-band observation, *Proceedings of the Conference on Weather and Other Information*, pp. 39-40, 2016.
- [6] A. Shimizu: Introduction of RGB composite imagery technique of MSG/SEVIRI in EUMETSAT, and application to satellite imagery of MTSAT-1R, *Meteorological Satellite Center Technical Report*, No. 51, pp. 7-9, 2008.